

Structural investigation of semicrystalline polymers

J. Molnár^{a,*}, Z. Zuba^a, Ö. Sepsi^b, F. Ujhelyi^b, G. Erdei^b, S. Lenk^b, A. Menyhárd^a

^a Department of Physical Chemistry and Materials Science, Laboratory of Plastics and Rubber Technology, Budapest University of Technology and Economics, H-1111, Budapest, Műegyetem, Rkp. 3. H. ép. I, Hungary

^b Department of Atomic Physics, Budapest University of Technology and Economics, H-1111, Budapest, Budafoki 8, Hungary



ARTICLE INFO

Keywords:
 Semicrystalline polymers
 Microscopy
 Polymeric structure investigation
 Supramolecular structure
 Morphology

ABSTRACT

This work demonstrates the most widely used characterization methods and techniques of the supramolecular and lamellar structure of semicrystalline polymers. Polarized optical microscopy (POM) equipped with a hot-stage (thermo-optical microscopy, TOM), brightfield microscopy (BF), darkfield microscopy (DF), digital image processing techniques, optical profilometry (OP), scanning electron microscopy (SEM), and atomic force microscopy (AFM) were used as investigation techniques. The same iPP grade was used with different sample preparation techniques to compare these methods. The advantages and drawbacks of the sample preparation and investigation methods were discussed. The results show how the introduced techniques could reveal different kinds of information, and it is also shown how the experimental techniques should be matched to the goals of a structural study.

1. Introduction

It is a well-known fact that plastics are essential materials used in several areas of our lives. Some of the most frequently used polymers are so-called semicrystalline materials. These materials always consist of amorphous and crystalline fractions. Usually, the crystallinity never reaches 100%, it ranges from 10 to 80%. The properties of these materials are dependent on the complex crystalline structure [1–14]. Consequently, studying the crystalline structure and morphology is highly the focus of many research studies.

Sample preparation is a critical issue for making evaluable images, therefore it should always be done with great care. The ideal technique always depends on the information we want to acquire from a sample and on the selected investigation technique. In the case of polymers, optical microscopy (OM) techniques like darkfield microscopy (DF), polarized optical microscopy (POM) usually do not require unique sample preparation methods or pre-treatments, and the structure of the “as-received” sample can be studied easily. The sample can be a thin slice made by a microtome, a fracture surface, or a thin polymer film crystallized in a laboratory press or between a slide and a cover plate in a hot-stage. In most cases, the crystalline morphology is studied using a thin film, in which the spherulitic structure is well discernible. The

techniques which allow the study of the samples in much larger magnifications (e.g., scanning electron microscopy (SEM), atomic force microscopy (AFM)) or the ones in which the surface of the samples characterized (e.g., optical profilometer (OP), AFM) usually require special pre-treatments. These sample preparation methods will be discussed further in the related sections.

1.1. Optical microscopic techniques (OM, DF, POM, TOM)

Many versatile characterization methods exist to examine polymers’ crystalline structure from the lamellar to the supramolecular scale. OM is the most convenient and frequently used technique for the investigation of the spherulitic system. The physical limitation of resolution is about 200–250 nm depending on the wavelength of the light source of the microscope and numerical aperture. Its primary advantage is that it is fast, relatively cheap, easy to use, reliable, and provides useful information about the supramolecular structure [15]. Using this technique, usually, the size and the shape of structural units (e.g., supramolecular structures, skin-core structure, inhomogeneities in the sample) are studied. Information on the local optical properties like the origin of light scattering, especially in DF, or the molecular orientation and the local refractive index in the case of POM can obtain [16–18].

Abbreviations Abbreviation Explanation: AFM, Atomic force microscopy; BF, Brightfield microscopy; DF, Darkfield microscopy; DOM, Digital optical microscopy; OM, Optical Microscopy; OP, Optical profilometry; POM, Polarized optical microscopy; SEM, Scanning electron microscopy; TOM, Thermo-optical microscopy.

* Corresponding author.

E-mail address: molnar.janos@mail.bme.hu (J. Molnár).

<https://doi.org/10.1016/j.polymertesting.2021.107098>

Received 15 January 2021; Accepted 28 January 2021

Available online 30 January 2021

0142-9418/© 2021 The Author(s). Published by Elsevier Ltd. This is an open access article under the CC BY license (<http://creativecommons.org/licenses/by/4.0/>).

POM is handy in studying the process of polymer crystallization because of the possibility of using a hot-stage in which the temperature of the crystallization is controlled. The hot-stage POM, also called thermo-optical microscopy (TOM), is a convenient way to study the crystallization's kinetics since the crystal evolution as a function of time and temperature can be recorded during the run of a temperature program [19]. Many types of instruments and techniques exist to enhance the contrast in OM [20]. For example, DF can be used to improve the contrast in highly scattering samples. Among the contrast enhancement techniques, POM is used most frequently in studying the polymer molecules' orientation and supermolecular structure [18]. Using crossed polarizers, the birefringent nature of crystalline parts forming in the non-birefringent amorphous melt offers high contrast because only those regions are visible in POM, which changes the polarization state of the light. Illuminating an anisotropic crystal with white light will appear colored between crossed polarizers. These interference colors are due to the unequal transmission of the white light's component wavelengths. The analyzer absorbs particular wavelengths depending on the amount of retardation produced in the light by its prior passage through the crystal [21]. The degree of transmission in the case of crossed polarizers is dependent on the path difference produced during the passage and on the wavelength of the light [22]. During the examination of polymers with a POM, we took advantage of this phenomenon using a so-called first-order plate, also called as full-wave plate or lambda plate. This plate is usually used to enhance the contrast in weakly birefringent specimens and to determine the sign of the birefringence. This plate is also made of a birefringent material and generates a fixed optical path difference around 560 nm [21]. Because of the ~560 nm retardation, only the ~560 nm wavelength light remains plane-polarized and absorbed by the analyzer, which yields a magenta color. Usually, this magenta color is the background color in POM. This color is also called sensitive violet because the human eye easily distinguishes it from the other interference colors associated with retardation, which is slightly more (yellow) or less (blue) than ~560 nm [21]. Accordingly, the study of the crystallization process in a quiescent melt or at other conditions and the study of the spherulitic structure and the formation of spherulites is possible as well [1,19,23,24]. The reliability of this technique decreases with increasing sample thickness. To gain valuable results, the samples should be thin to allow the 2D analysis of individual spherulites. In thick samples, spherulites can form one above the other and below which prevents the observation of spherulite boundaries and the determination of spherulite numbers and sizes are difficult if not impossible at all.

Many examples can be found in the literature using POM to investigate the semicrystalline structure of polymers. Androsch et al. [25] applied POM with fast scanning chip calorimeter to investigate homogenous crystal nucleation in polymers. Varga et al. studied the different types and modifications of polypropylene spherulites using POM [1,19,23]. POM also allows the classification and identification of different types of spherulites based on the difference between the birefringence of the various crystalline modifications (Table 1) [24]. What stands out in the table is that the birefringence of different types of spherulites can be positive, negative, or mixed. The birefringence value of spherulites is determined by the orientation of lamellae (more precisely the polymer chains within the lamellae) in the spherulites and can be defined as the follows:

$$\Delta n = n_r - n_t \quad (1)$$

where n_r and n_t denotes the spherulites' radial and tangential refractive index, respectively [26].

The simplicity of POM and TOM supported the widespread application of these methods. Digital cameras are equipped with most TOM or POM microscopes, which opened a new field, the digital optical microscopy (DOM). In this technique, the principles are the same as in the conventional OM, but the microscope is slightly different. The image is

detected by CCD or CMOS cameras and not by the human eye. With digital image processing techniques, the limitations of depth of field and field of view can be easily overcome at a given magnification. These techniques usually stitch images taken at different focal distances and in different regions [16,27]. Most of these microscopes can assign the location coordinates to the sharp pixels to create a 3D image. They are convenient to use and can be used to perform various 2D and 3D measurements quickly. Thanks to automatic image processing, it is even possible to automatically evaluate images, such as automatically detecting different shapes and structures (e.g., spherulites, fillers) and automatically determining the dimensions and number of these (e.g., nucleus density, spherulite size).

1.2. OP

Another frequently used technique for the investigation of spherulites is optical profilometry (OP), also known as white-light interferometry. In OP, a light beam of short coherence length passes through a beam splitter, directing the light to the sample and the reference mirror. The light reflected from the two surfaces recombines, a pattern of interference fringes forms. During the measurement, the sample's surface scanned vertically, and the height of each point is determined. It is also a non-contact, non-destructive method, suitable for characterization of the surface roughness on the sub-micrometer scale measuring the surface height at a given lateral position with high speed and accuracy. The achievable lateral resolution is similar to optical microscopes, but the height resolution is in a few nanometer range. Another advantage is that sample preparation is generally unnecessary [28], and even a simple fractured surface can be investigated.

It should be noted that for the investigation of the crystalline structure, etched samples are needed sometimes. The etching is a frequently used method to make the crystalline structure more visible and raise the amount of information obtained from the samples by different microscopic techniques with high magnification. In the etched samples, the amorphous layer is partially removed (selectively dissolved) so that the remaining crystalline fraction determines mostly the morphology of the surface. As a result, spherulites and other supermolecular formations can be studied with devices that map the surface microstructure. Special solvents are usually used for semicrystalline polymers, which dissolves the amorphous regions much better than the crystalline phase. Therefore the topology of the remaining structure becomes more visible after the treatment of the surface. Table 2 shows examples of the most frequently used etchants applied for different polymers. For instance, for polyolefins, Olley, and Bassett's permanganic etching solution is used to investigate the supermolecular structure [16,29].

1.3. SEM

The analysis of the subspherulitic or lamellar structure requires a large resolution [31,32]. To make high-resolution images from the lamellar structure, scanning electron microscopy (SEM) can be used. Etching of the samples is inevitable to reveal the crystalline structure on the surface. If nonconductive materials are analyzed, conductive coatings are required to prevent the samples from charging up in the electron beam. This problem is even more severe in the case of organic materials, like most of the polymers. A highly focused electron beam is necessary to achieve a large resolution, which leads to a higher energy density on the surface, which can damage the sample. To reach higher magnifications, low energy SEM should be used. Thanks to the low accelerating voltages, the beam damage is reduced, and sometimes the need for conductive coating is also preventable [33]. However, most of the conventional polymers are good insulators therefore conductive coatings are usually needed [16]. In most cases, the conductive coating means a thin surface layer of Au, Pt, W, and Ti [31]. Using SEM, the crystallization of polymers, fracture surfaces, and phase separation in polymer blends can be studied.

1.4. AFM

Atomic force microscopy (AFM), belonging to the family of scanning probe microscopes, is one of the best techniques for the characterization of the lamellar structure of semicrystalline polymers [33–35]. The most common purpose of the investigation is the visualization of the sample morphology. The experimental studies sometimes require etching to remove the structureless topmost layer to visualize the fine lamellar morphology of the polymer [4,35,36]. However, the growth of lamellar and subspherulitic structures can also be visualized *in situ* without the need of etching [37,38]. More sophisticated measurement modes enable the characterization of the local nanomechanical properties of the sample. During the measurement, a cantilever with a microfabricated tip deflects when interacting with the sample surface. The microscope registers the interacting force as a function of the distance and calculates nanomechanical properties like modulus or adhesion. For the latter, one uses different theoretical (e.g. Derjaguin-Müller-Toporov or Johnson-Kendall-Roberts) models depending on the nature of the tip and sample [39]. The combination of imaging and determining mechanical properties at the nanoscale has particular interest for semicrystalline polymer because not only the nanomechanical properties but also the number, shape, and spatial arrangement of the crystalline component contribute to its macroscopic material properties [35,40]. Furthermore, when AFM is combined with a high-sensitivity conductive working mode (C-AFM), then local currents can be studied simultaneously with morphology [41–43].

In this paper, the imaging techniques mentioned above were used to characterize the morphology of the samples prepared by different sample preparation techniques and made from the same well-known polymer: isotactic polypropylene (iPP). Our goal is to show the usability and limitations of these techniques and show what necessary conclusions can be drawn about semicrystalline polymer structures using these techniques.

2. Sample preparation and characterization

Isotactic polypropylene (iPP) was selected as a model material. Its extensively studied well-known crystalline structure makes it an ideal candidate to present the strengths and limitations of the techniques. A commercial polypropylene, Tipplen H 649 F H, with MFR = 2.5 g/10 min (230 °C, 2.16 kg) from MOL Group (Hungary), was used. The neat polymer and its two nucleated versions containing different nucleating agents were used to prepare the samples. The nucleating agents were added to polypropylene to change the structure. One of them is a clarifier, a soluble sorbitol derivative, an organogelator, namely 1,2,3-trideoxy-4,6:5,7-bis-O-[(4-propylphenyl)methylene]nonitol, marketed as Millad NX8000 and produced by Milliken Chemical Company (USA). It was added to the matrix in the amount of 4000 ppm to create a so-called microcrystalline structure. The other nucleating agent is a heterogeneous nucleating agent, namely NA21E produced by Adeka-Palmarole (France). From this nucleating agent, 1000 ppm was mixed to the polymer to create a microspherulitic structure. Homogenization of the premixed compositions of polypropylene matrix and nucleating agents was ensured by molten state extrusion with a Brabender Plasti-Corder 42/7 twin screw extruder. Compounding was carried out with 210–220–225–230 °C barrel temperatures at 50 rpm screw speed. The extruded melt strands were cooled in air and granulated. From the granules, 1 mm thick plates were injection molded using a DEMAG IntElect electronic injection molding machine. The barrel zones were set to 210–220–230–230 °C, and a constant mold temperature of 40 °C was used during the production of all samples. During the injection molding, 500 bar holding pressure and 60 cm³ s⁻¹ injection speed were used. From the 1 mm thick injection-molded plates, samples with a thickness of 20–50 µm were prepared with LEICA REICHERT JUNG Polycut microtome at –20 °C.

Plates with 2 mm thickness were also made in a laboratory press,

crystallizing neat iPP at 150 °C for 10 h to obtain large spherulites. First, the amount of iPP granules required to fill the press frame was placed in the center of the laboratory press heated to 200 °C. Three deaeration steps were inserted while closing the compression molding machine to avoid air bubbles in the samples. After it was closed, it was cooled down to 170 °C with cooling water, and then it was allowed to cool down to 150 °C. From this point, the sample let to crystallize at 150 °C for 10 h. After 10 h, the temperature control was switched off and waited until it cools down to room temperature. From the 2 mm thick plates, thin films were made with a microtome at –20 °C, and the samples were also made by breaking it to examine the structure on the fractured surface. The crack follows the spherulites' boundary zones while breaking the sample, therefore revealing the spherulitic structure.

To obtain well-developed spherulites, thin samples were also made from the native polymer between glass slides using a hot-stage at 134 °C, 136 °C, and 138 °C for different periods of time determined by the radial growing speed of the spherulites at the given temperature. To take good quality images and not bring any contaminants into the sample, which could act as a nucleating agent, great care must be taken to ensure that everything is clean and dust free during the sample preparation. Prior to use, the microscope slides and cover glasses should be ultrasonically washed to remove dirt from their surface. The first step is to place a small piece of polymer about 5 mg between two glass plates. After that, the sample is placed on a heatable stage and heated until the sample melted. In the case of iPP, 220 °C is usually used. After the complete melting of the sample, a weight can be placed on the top, and the weight can be pressed gently. The compression load should keep on during the entire further procedure. When the sample has reached the predefined temperature, the heating unit switched off, and the sample was cooled down spontaneously. The two glass plates should be separated after the cooling, and a thin cover plate is placed on the top, and the entire procedure is repeated. After this process, a 5–10 µm thick sample can be obtained between the microscope slide and the cover glass. This sample is ready to investigate with a microscope, but to create the required crystal structures in the thin film, isothermal crystallization can be performed in a hot-stage unit. This unit can be placed under the microscope so that the evolving structure can be continuously monitored. It is essential to always erase the sample's thermal and mechanical prehistory before the isothermal crystallization step. In the case of iPP, this can be done with an isothermal step at 220 °C for 3 min. At such a high temperature, due to the high mobility of the polymer chains, the regular crystalline units and orientation of the polymer can disintegrate, therefore the thermal and mechanical prehistory is erased.

With OM in reflection mode, OP, SEM, and AFM, the sample's surface is examined. To investigate the crystalline structure on the surface of semicrystalline polymer thin slices, fractured surfaces, etc., the amorphous layer should be removed from the surface of the samples to reveal the spherulitic and lamellar structure. Potassium permanganic etching is usually used for polyolefins, according to Basset et al. [30]. The etching time was 24 h at room temperature for all samples in our case.

Table 3 provides an overview of microscopic techniques used to study the different levels of structure, the instrument we used, and the accessories occasionally applied in the study.

3. Results and discussion

Fig. 1 shows a 3D DOM image from the fracture surface of iPP crystallized in a laboratory press at 150 °C for 10 h. The shape and sizes of well-developed spherulites around 100 µm can be seen. The sample was cooled to room temperature, where the fracture was performed. Due to the relatively low temperature of fracture, no pronounced plastic deformation appeared, thus the spherulites were not plastically deformed, and their original shape can be easily observed. We have to note that such highly crystalline samples prepared by high-temperature annealing usually contain small cracks and voids formed inside the

Table 1

Different spherulite types and their birefringence [1,23,24].

Spherulite type	Crystal modification	Birefringence	Crystallization temperature [°C]
I	α	weakly positive	<134
II	α	weakly negative	>138
Mixed	α	mixed	134–138
III	β	negative	110–128
IV	β	negative	128–140

Table 2

Etchants for different polymers [16].

Polymer	Etchant
PE	hot carbon tetrachloride, benzene, or toluene
PE, PP	xylene or benzene
Melt crystallized PE	95% fuming nitric acid (80 °C)
PE, isotactic PP	potassium permanganic etching Basset et al. [30]
Nylon 6, and 6,6	aromatic and chlorinated hydrocarbons
Cellulose acetate	acetone at –50 °C, then cold ethanol
Polycarbonate	triethylamine, chloroform vapor

sample due to the volume contraction during the crystallization process. Consequently, the impact resistance of these samples is usually relatively low [44].

Fig. 2a shows a DOM image of a microtomic slice from the same sample shown in Fig. 1. The image was also made with a 3D stitching technique, which can be used to create a sharp image of the whole slice (roughly 1.8 mm × 1.8 mm). In the figure, the cross-section of the well-developed hundreds of μm large spherulites can be observed. We can also notice that the sample is cracked and at some places, the spherulites are “missing” from the slice. Microtomic slices, especially in samples crystallized at high temperatures, often fragmenting during cutting. The cracks initiate on the weak points in the boundary zones of the spherulites. Fragmentation and any damage of the sample are more observable in DF images (Fig. 2b), where due to the separation of spherulites, light is highly scattered from the gaps. Therefore the regions which are separated will be bright in the DF microscope. In Fig. 2b, it can also be seen that not only the edges but the spherulites itself also scatter the light considerably.

In addition to an ultramicrotome, thin slices are also made by crystallizing samples between microscope slides. Fig. 3 shows images made by different techniques (POM, DOM, BF, DF) from the same isothermally crystallized sample (136 °C) and the same area. Fig. 3a is a typical POM image from well-developed iPP spherulites using a lambda plate. The interference colors make specific Maltese-cross patterns in the spherulites. The different kinds of spherulites (like Maltese cross, ring-banded)



Fig. 1. DOM image of spherulites on the fracture surface of sample crystallized in a laboratory press at 150 °C for 10 h.

and the explanation for this phenomenon can be found in the literature [24,45,46]. The spherulites grow uniformly in all directions and finally impinge upon each other forming polygonal units. Several factors influencing the shape of the spherulitic boundaries, useful information can be obtained from the investigation of it [47]. In Fig. 3a, straight and curved borders can be recognized. Since the crystallization is isothermal and the same crystal modifications are growing, the spherulites' radial growth rates are the same. In this case, the straight boundaries mean that the nucleation occurred at the same time, while the curved boundaries mean the opposite, namely that the spherulite at the concave side formed later. If the growth rate is known, the time difference can be calculated from the shape [47,48]. The separation of the spherulite borders can also be recognized in this case as dark lines between the spherulites. The reason is different than in the case of microtomic slices. The gap between the spherulites is due to contraction during the crystallization, as in the samples crystallized in the laboratory press. At the end of the crystallization near the glass slide, there is not remaining enough polymer to fill up the whole place, therefore thin gaps are formed. This appears only on the surface of the spherulitic samples. Fig. 3b is recorded with a DOM in reflection mode when the surface topology of the sample can be studied. This technique does not give any information about the birefringence and, therefore, the type of crystal modification of the spherulite. However, the gaps between the spherulites, the damages on the surface, etc., are more recognizable. Fig. 3c is made with the same technique as 3 b but with polarizers without a lambda plate. It can be seen that better contrast in the reflection mode also can be achieved using a polarizer.

Fig. 3d shows the BF image (transmission mode), and Fig. 3e shows the DF image. These images are made from the same sample but after removing the cover glass. The sample has been damaged during the removal of the cover glass leaving marks on the spherulites' surface. The DF image (Fig. 3e) provides additional information about the origin of the light scattering in the sample. Using this technique, the gaps, the scratches, and anything that causes light scattering is more pronounced than the previous methods.

The degradation of the spherulites at high temperatures can also cause similar black lines at the boundaries, as in Fig. 3a, but these lines are much more disordered and are not only observable at the edges of

Table 3

The investigation techniques used in this study.

Technique	Structural level	Instrument	Accessories
BF, DF POM, TOM	Spherulites	Olympus BX51 MPLFLN-BD	
	Spherulites	Leitz dialux 20	Mettler FP82 hot-stage,
		Zeiss Axioscope	λ -plate
DOM OP SEM	Spherulites	Keyence VHX 5000	
	Spherulite	Bruker ContourG K0-X	
LEO	Lamellar-spherulite	Jeol JSM-6380 LA	
	Lamellar-spherulite	Zeiss LEO 1540 XB	
AFM	Lamellar-spherulite	Bruker Dimension Icon AFM in Peak Force Tapping mode	Bruker ScanAsyst-Air probe

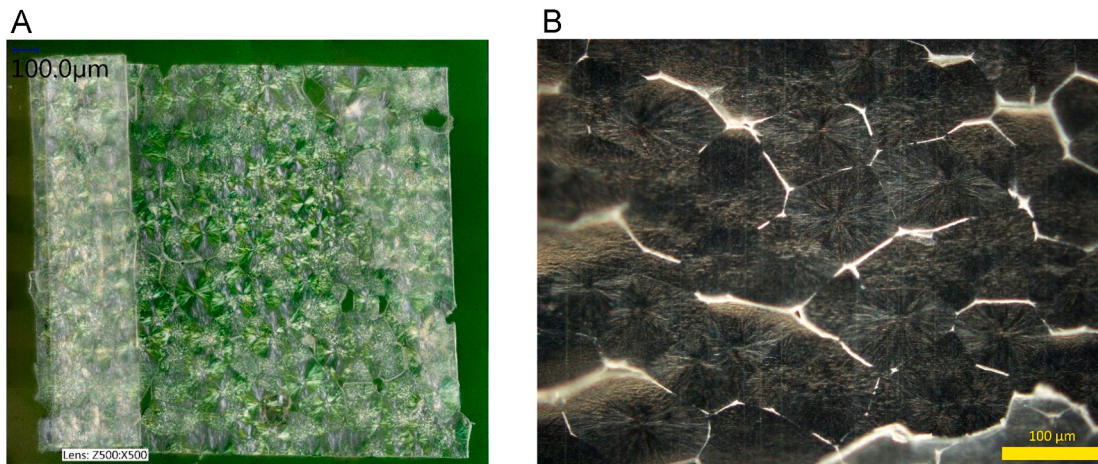


Fig. 2. a) DOM and b) DF image from a 5 μm thin slice made using a microtome. Sample made from neat iPP crystallized in a laboratory press at 150 $^{\circ}\text{C}$ for 10 h.

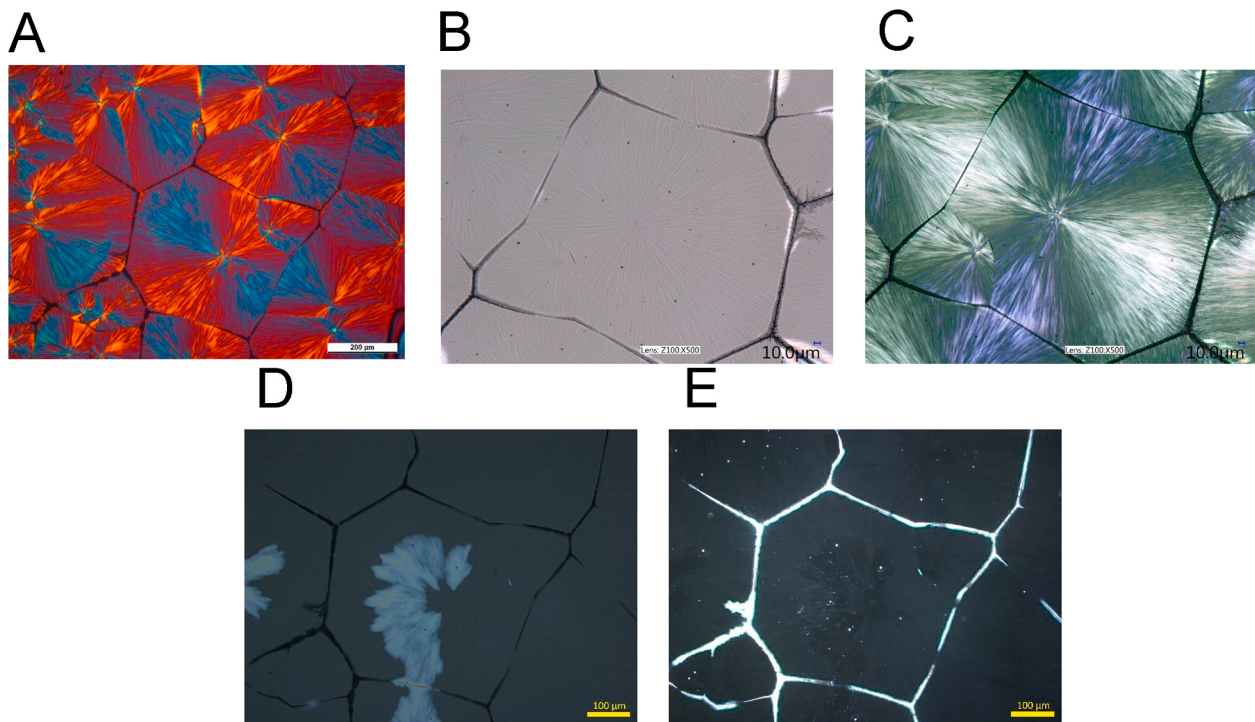


Fig. 3. a) POM with lambda plate (Leitz) b) DOM (Keyence), c) POM (Keyence), d) BF (Olympus), e) DF (Olympus) image from spherulites crystallized at 136 $^{\circ}\text{C}$ for 3 h between glass slides.

the spherulites but also inside them (Fig. 4). Due to degradation, the crystal front cannot spread uniformly, this causes the disordered spherulitic boundaries.

On the BF and DF images below (Fig. 5), we can observe that no significant light scattering occurs at the borders where the spherulites do not separate from each other. In Fig. 5b, we can also observe that spherulites itself significantly scatter light. It can be said that inside the sample, in the bulk phase, where the spherulite borders do not separate, the light scattering originates from the spherulites. In the literature, many articles deal with explanation and the description of the light scattering of spherulites [49–56].

To get a more accurate picture from the sample's surface morphology on the spherulitic level, a suitable method is to use OP. With OP, we can take a detailed picture of the surface, for example, from the gaps between the spherulites. Fig. 6 shows 3D OP micrographs from the same sample and area shown in Fig. 3. Fig. 6a shows the detailed spherulitic

surface structure and the damaged regions of the sample's surface. Due to the sample thinning caused by this damage, spots are visible in Fig. 3d and e. In Fig. 6b, the gaps between the spherulite borders can be seen. Fig. 6c shows an OP micrograph from the etched surface of the spherulitic cross-section of the injection-molded neat iPP sheet. Spherulites of approximately 20 μm and the structure of the surface are well observable. In these OP images, the lamellar structure is also visible.

With POM, the different crystal modifications can be easily distinguished and identified according to Table 1. In Fig. 7, a POM image from β -spherulitic inclusion in the field of α -spherulites can be seen. The β -spherulites have more significant birefringence than the α -spherulites and scatter the light more, which results in a unique image: the β -spherulites sort of shine in the middle of the α -spherulites in polarized light. The contour of the spherulitic boundaries around β -spherulites is curved because the growth rate of spherulites of β -modification at this crystallization temperature (134 $^{\circ}\text{C}$) exceeds the growth rate of

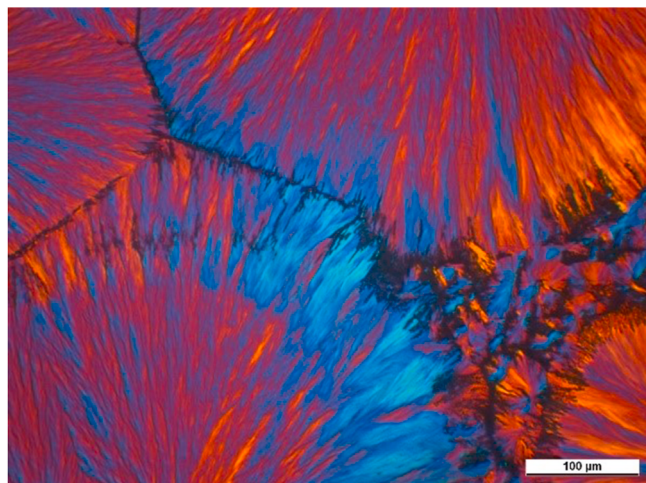


Fig. 4. POM image from the degradation of spherulites crystallized at 138 °C for 6 h between glass slides.

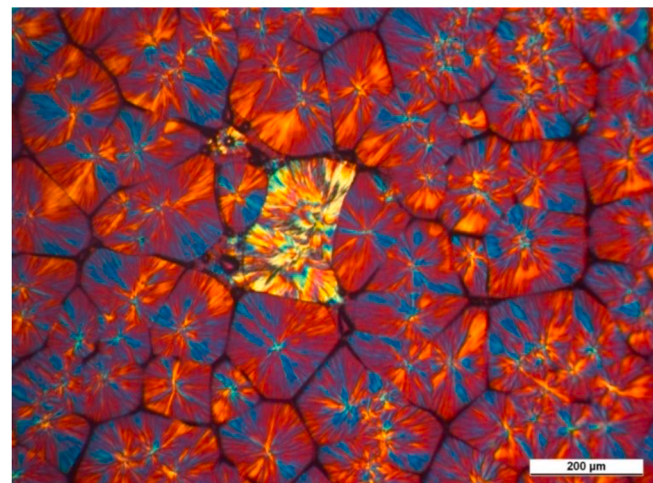


Fig. 7. POM image from β -spherulitic inclusion in the field of α -spherulite taken from sample crystallized at 134 °C for 2 h between glass slides.

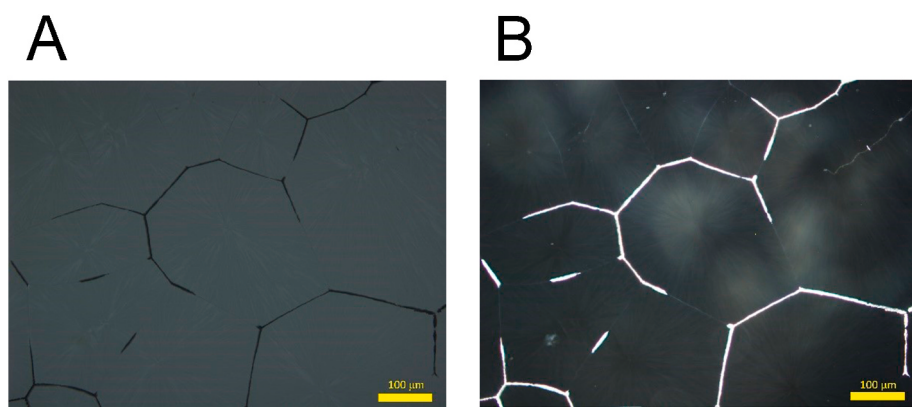


Fig. 5. a) BF and b) DF images from spherulites crystallized at 138 °C for 6 h between glass slides.

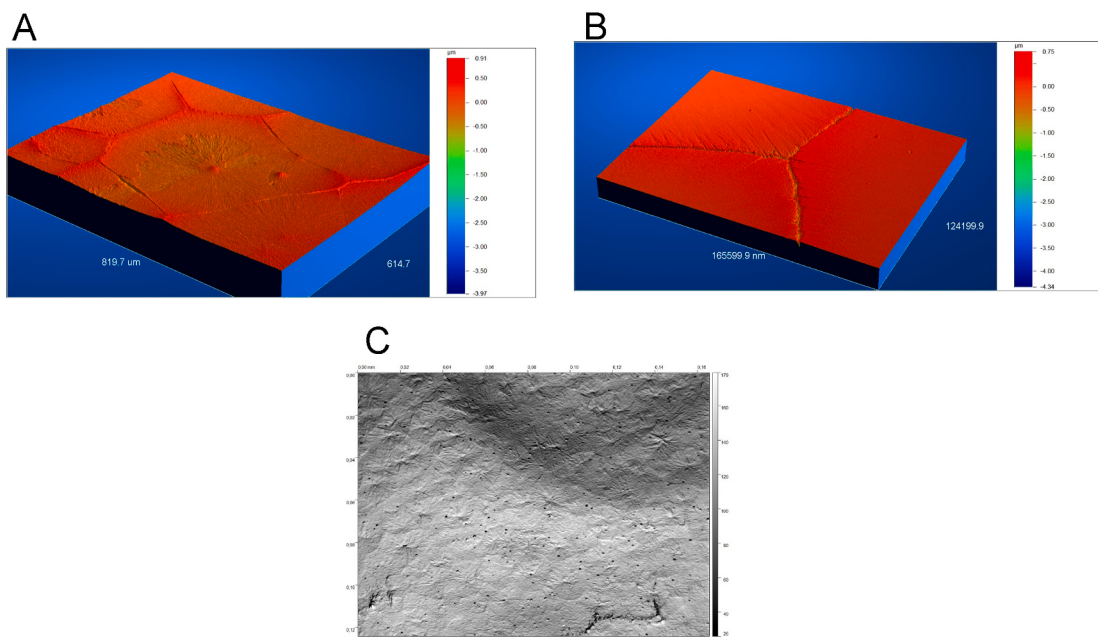


Fig. 6. OP micrographs from the a) spherulitic structure and b) the gap between spherulites formed at 136 °C for 3 h between glass slides. Figure c) shows the etched surface of a thin slice made with microtome from an injection-molded neat iPP sheet.

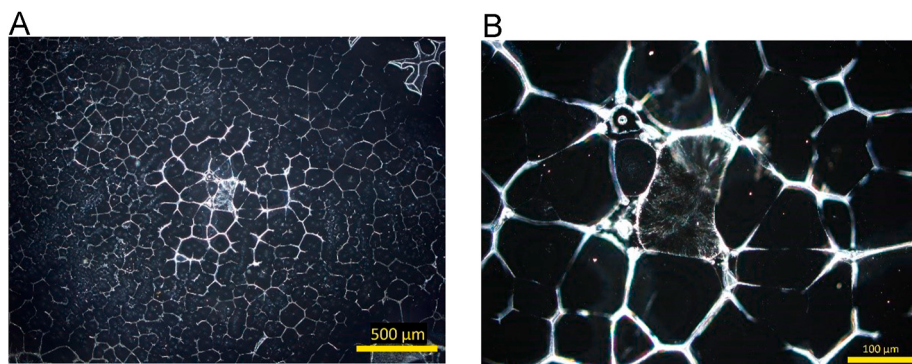


Fig. 8. DF images with 5x a) and 20× b) magnification from β-spherulitic inclusion in the field of α-spherulite taken from sample crystallized at 134 °C for 2 h between glass slides.



Fig. 9. 3D DOM image from the fracture surface of iPP plate crystallized in a laboratory press at 150 °C for 10 h.

α-modification. If different crystal modifications are growing together, spherulites' contour can be very diverse from circle to a straight line, hyperbola, limacon of Pascal, etc. [47]. Based on Table 1, the β-spherulites are type IV, and the α-spherulites are mixed.

Using other microscopic techniques like DF or DOM, the different spherulite types can also be recognized due to the different birefringence and, therefore, light scattering of different types of spherulites. In Fig. 8, DF images made at different magnification can be seen from the same sample and the same area as in Fig. 7. The reason is the same. The β-spherulites have larger birefringence values than α-spherulites. The β-spherulites scatter the light more, and they are brighter than the α-spherulites. It can be seen in Fig. 8a that the environment of β-spherulites is much brighter due to the intense light scattering.

β-Spherulites can be detected even on simple DOM images. Fig. 9 shows a 3D DOM image from the fracture surface of iPP sheet. The brighter spherulite in the middle is a β-spherulite surrounded by α-spherulites. However, with DOM and DF, the proper identification of the spherulites is not possible because these techniques do not give information about the sign and the value of the birefringence.

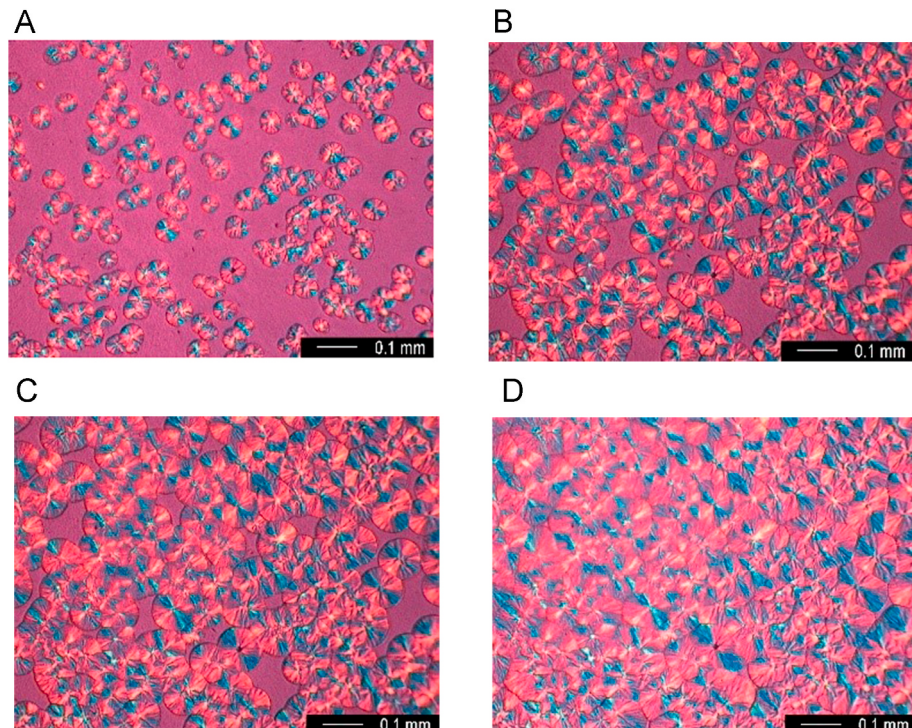


Fig. 10. POM images (using lambda plate) of the polycrystalline structure of iPP during crystallization at 135 °C at different crystallization times [59].

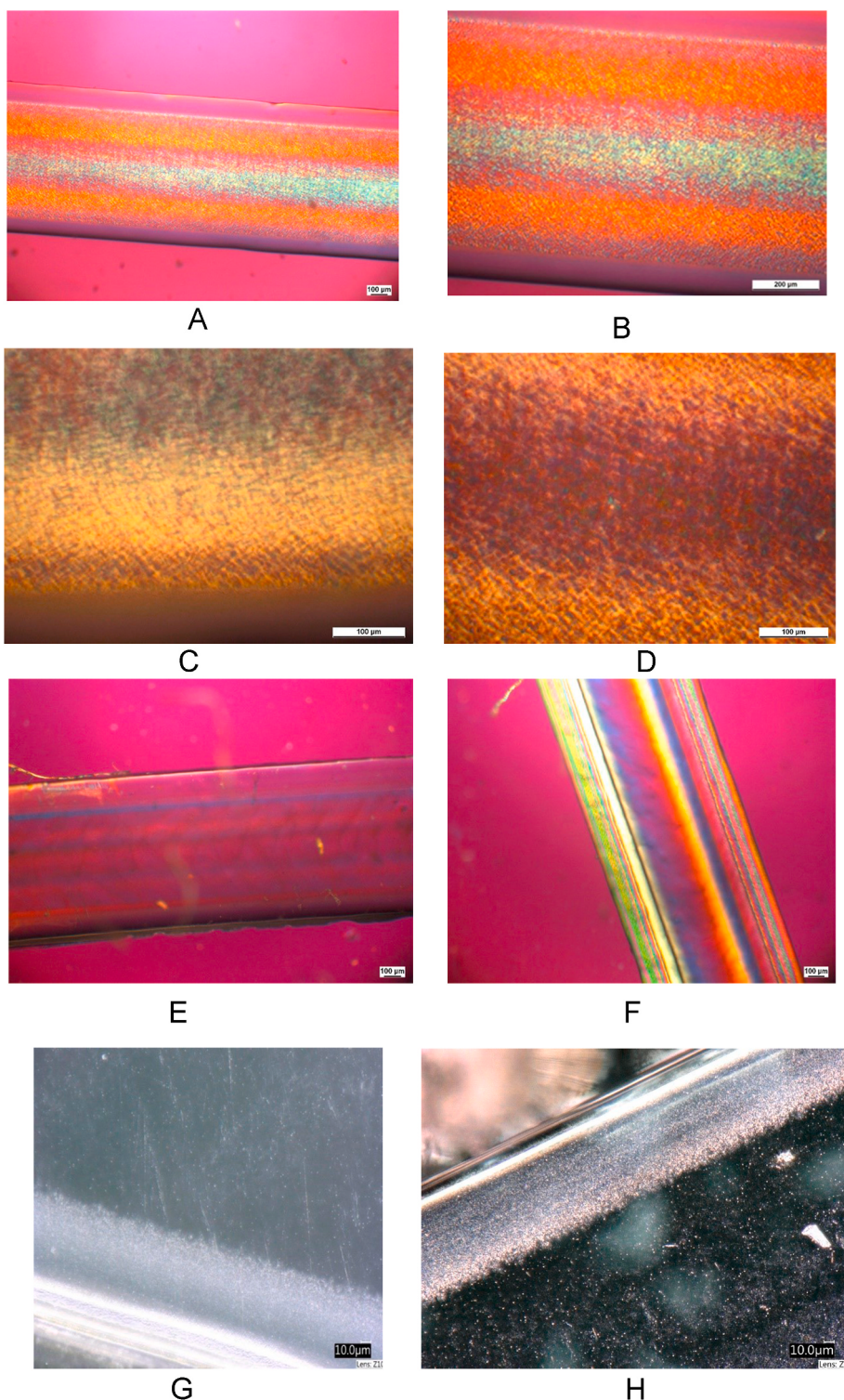


Fig. 11. POM and DOM image from the cross-section of the injection molded and etched samples made with a microtome. POM image of neat iPP with a) 50 \times and b) 100 \times magnification. POM image with 200 \times magnification from the c) skin and the d) core structure. POM image with 50 \times magnification of sample containing e) 1000 ppm NA21E and f) 4000 ppm NX8000 nucleating agent. DOM image of the oriented skin layer g) before and e) after sputtering.

With POM equipped with hot-stage, the final crystal structure and spherulite development are easy to observe and monitor during thin layer crystallization. Typical POM (with lambda plate) micrographs recorded during the crystallization can be seen in Fig. 10. With this technique, the linear growth rate of the spherulites at a given temperature, the final nucleus density, and in some cases, the rate of nucleation can be determined by taking images at given intervals. These pieces of

information are crucial for several kinetic calculations and polymeric structure evolution simulations [57]. Another common application of POM with hot-stage in the field of polymer crystallization is for the qualitative investigation of nucleating agent efficiency and solubility [58].

Fig. 11 shows the skin-core structure of injection-molded specimens. Figs. 11a and b shows the typical skin-core structure for an iPP sample

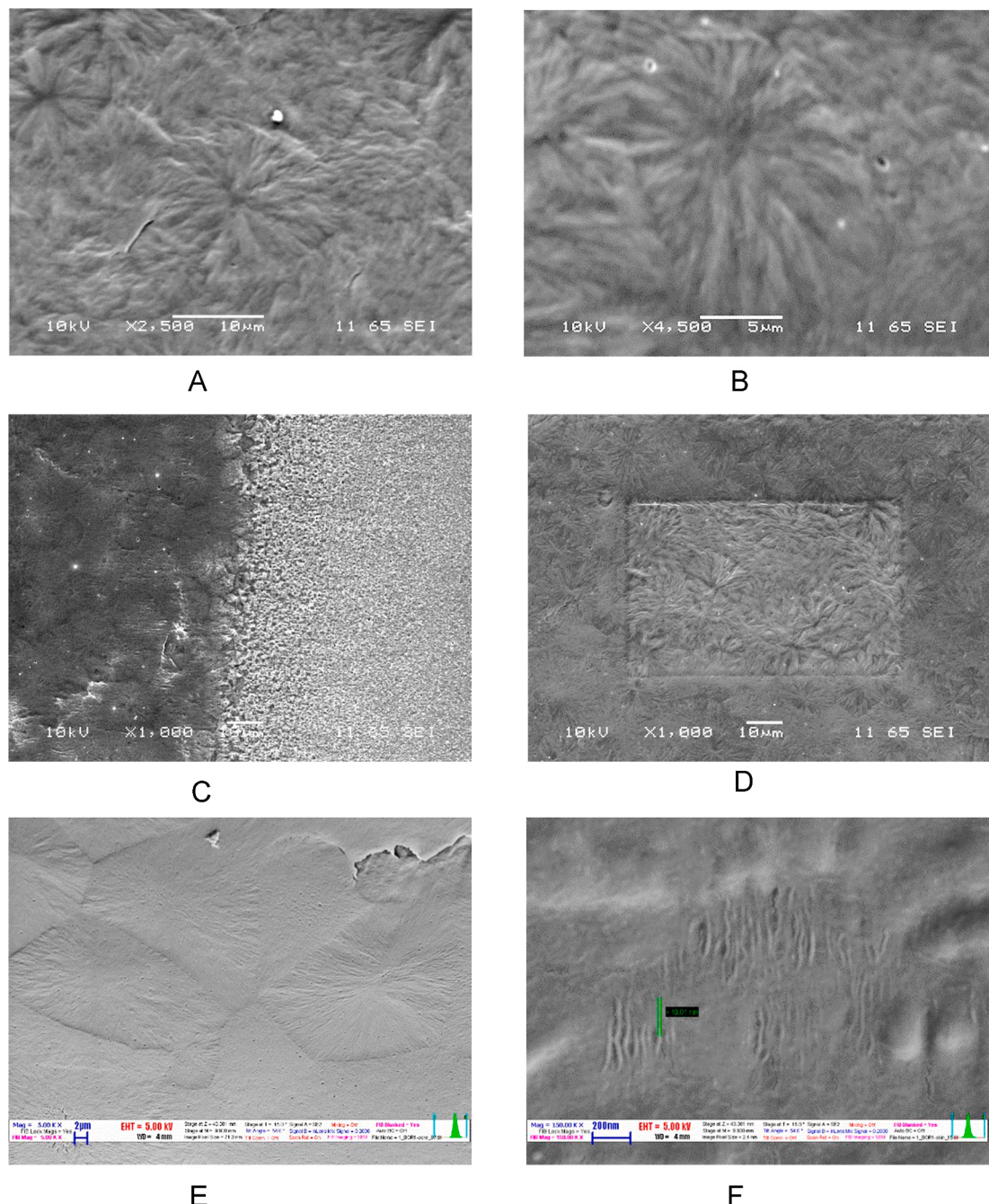


Fig. 12. SEM image from the spherulitic and lamellar structure of injection molded neat iPP samples. Images were taken from the etched surface of the slices made with a microtome a) 2 500x and b) 4 500× magnification of spherulites with the effect of lamellae thickening, c) 1 000× magnification from the skin-core structure, d) image from the electron beam degraded area, e) low energy SEM image of spherulites at 5 000× magnification without the effect of lamellae thickening f) the thickness of lamellae at 150 000× magnification.

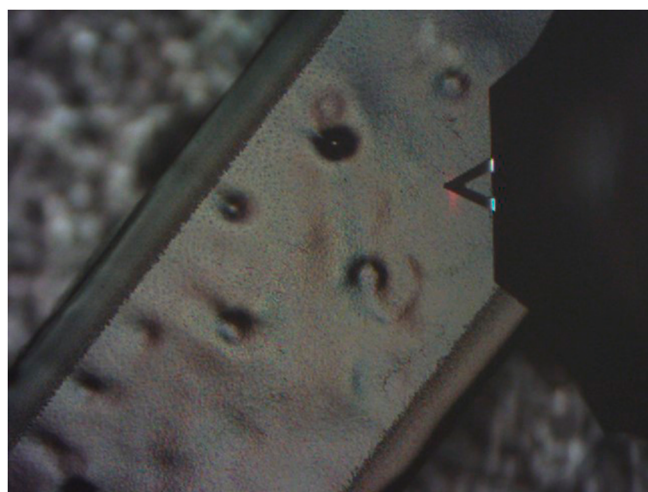


Fig. 13. The location of AFM cantilever above the injection-molded iPP sample made with microtome.

without a nucleating agent. [Fig. 11c](#) shows the skin and [Fig. 11d](#) the core structure. During the injection molding process, the different temperature and shearing conditions in the cross-section result in different crystalline structures and supermolecular structures. Due to rapid cooling, the outermost skin layer is solidifying in a not birefringent amorphous state, and therefore its color does not change, remains sensitive violet. The core cools slower than the skin, there is enough time for the polymer chains' relaxation, and in quiescent conditions, spherulites form. Due to the temperature gradient during cooling, the largest spherulites can develop in the center of the sample, and the farther we get from the center of the sample, the smaller the spherulites are. It can also be seen on the POM images that the spherulites' size and color also change in the cross-section of the sample. Different types of spherulites with varying interference colors formed due to the temperature and shear gradient during the injection molding. [Figs. 11e and f](#) shows the POM images of samples with nucleating agents. With rapid cooling and in the presence of nucleating agents, the supermolecular units are so small that they cannot be studied and identified with the techniques used so far and described above. Due to the size reduction of the supermolecular units, these samples scatter the light less, therefore they are transparent. In [Fig. 11e](#) and [f](#), the spherulites are so small that they can no longer be examined by light microscopy. [Figs. 11g and h](#) shows DOM images from the skin layer of the neat polymer sample. The samples' skin scatters the light more than the center, caused by the cylindrical supermolecular structure formed in the sheared melt. In [Fig. 11h](#), the skin layer structure is more observable than in [11 g](#) because, in this case, a thin gold layer on it enhances the contrast on DOM images.

When supermolecular structures are no longer observable by light microscopy, SEM or AFM are used most in polymer physics research. In SEM images ([Fig. 12](#)), in addition to the spherulitic structures, the lamellar structure can also be studied. On the etched samples' surface, discrete spherulites, and the borders among them ([Fig. 12a and b](#)) and the skin-core structure ([Fig. 12c](#)) can be easily observed. It can be seen that the structure in the core is quite different from the structure in the skin, where small spherulites can be observed. SEM is a destructive technique. The electron beam channels a current onto the sample, which must be conducted away to prevent charge accumulation and degradation on the sample. Polymers are excellent insulators. Despite the different conductive coating, the surface degrades rapidly. [Fig. 12d](#) shows the effect of the electron beam on the gold layer coated sample. The electron beam warms up the sample's surface, degradation and partial melting occur, which changes the sample's crystalline structure during the investigation. Therefore, a new structure appears in the image. The larger the magnification, the stronger this effect. In [Fig. 12d](#),

the modified region of a previously examined area at larger magnification can be seen. Due to this effect, we are always moving towards lower to larger magnifications in a given area, and at large magnifications, the sharpness is adjusted next to the desired area of the examination not to degrade it. The degradation of the polymeric samples limits the achievable magnification. To overcome this problem, low energy SEM is usually used. [Figs. 12e and f](#) images made with low energy SEM. Low energy SEM enables the study of the original crystalline structure because the used electron beam does not have enough energy to melt the surface locally and induce recrystallization. In [Fig. 12e](#), the original spherulitic structure without lamella thickening can be observed. In [Fig. 12f](#), at 150 000 \times magnification, even lamellas can be studied without degradation.

To archive larger magnification from the surface structure than with SEM, AFM should be used. The following AFM micrographs were made from the center of injection molded samples. [Fig. 13](#) shows an example of the location of the cantilever above the sample.

AFM enables the study of the crystalline structure of polymers in detail without damaging it. [Fig. 14a](#) shows the discrete spherulites of neat iPP samples on the etched surface. In the lower right corner of the image, a well-developed rosette structure is observable. In [Fig. 14b and c](#), the lamellar structure, the dimensions, and also the branching of the lamellas can be studied. [Figs. 14d and e](#) shows images from the micro-crystalline structure of iPP using NA21E nucleating agent. The difference between the structure of the samples made with different nucleating agents is easy to observe. The lamellae using NA21E have formed on small particles instead of fibrils. The structure is not as oriented as we observed during the analysis of the sample made with the clarifier ([Fig. 14f](#)). In [Fig. 14f](#), the etched surface of the sample with 4000 ppm NX8000 nucleating agent can be seen. This type of nucleating agent is soluble in the polymer melt on elevated temperatures, and during the cooling process, it forms a network of nanofibrils. During cooling, the crystallization can take place on this network, and epitaxially growth microcrystalline structure can form. Due to the large surface area, the density of nuclei is significantly raised, which results in the formation of a microcrystalline structure. The lamellae are smaller, and the nanofibrils are more oriented due to the injection molding, which makes the localization of the lamellae oriented as well.

Using AFM, high-resolution 3D images can be captured like [Fig. 15](#) below, where the 3D image of the previously shown [Fig. 14e](#) is made.

4. Summary

In this work, the sample preparation methods and the most common imaging techniques for studying semicrystalline polymers presented. Neat iPP and iPP with two different nucleating agents were used to prepare samples with diverse supermolecular and lamellar structure. Structures created containing large spherulites to microcrystalline structures, like plates crystallized in a press, injection-molded samples, thin slices made with a microtome, and thin films crystallized between microscope slides. The importance and ways of etching, the precautions to be taken during sample preparation and testing of semicrystalline polymers were also discussed. BF, DF, POM, digital image processing techniques, OP, SEM, and AFM were used, and the phenomena observed with these techniques were discussed. At the specific investigation method, we explained the essential characteristics of these different samples. We have shown, through some examples, the most common structures that occur in the study of semicrystalline polymers and the phenomena associated with them like the typical characteristic of a spherulitic fracture surface, the shape of the boarders between the spherulites, the skin-core structure of injection-molded specimens, the different structure developing in the presence of heterogeneous and soluble nucleating agent, the characteristics of spherulites in different investigation methods, the birefringent nature of polymers and its effects, the different spherulite modifications or the effect of degradation on the images.

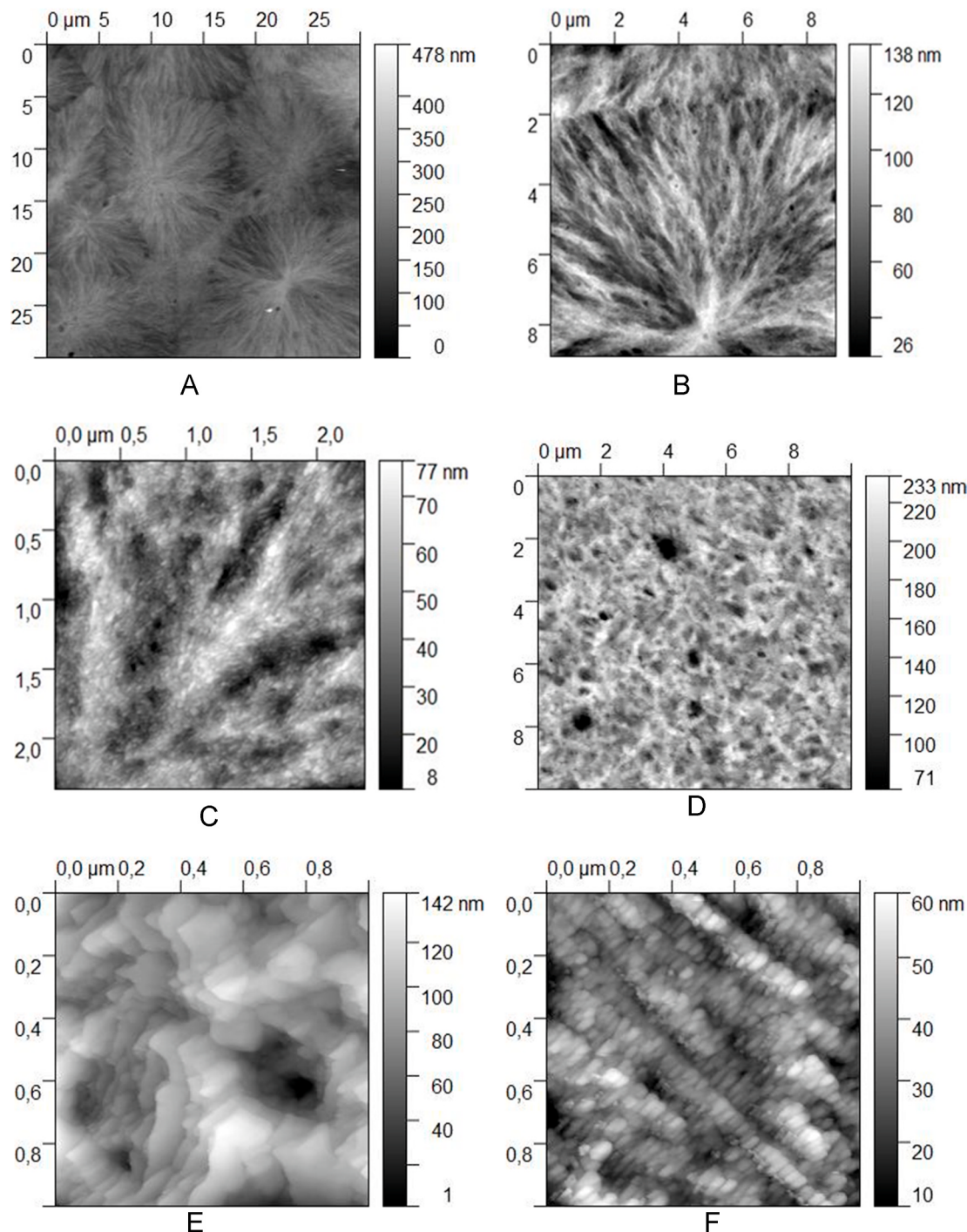


Fig. 14. AFM image from the supermolecular and lamellar structure of iPP samples. a), b), and c) shows the spherulites of neat iPP with increasing magnifications. d) microcrystalline and e) lamellar structure of a sample with 1000 ppm NA21E. f) microcrystalline structure with epitaxial growth on the surface of the fibrils of the NX8000 nucleating agent.

Data availability statement

The raw/processed data required to reproduce these findings cannot be shared at this time as the data also forms part of an ongoing study.

Declaration of competing interest

The authors declare that they have no known competing financial interests or personal relationships that could have appeared to influence the work reported in this paper.

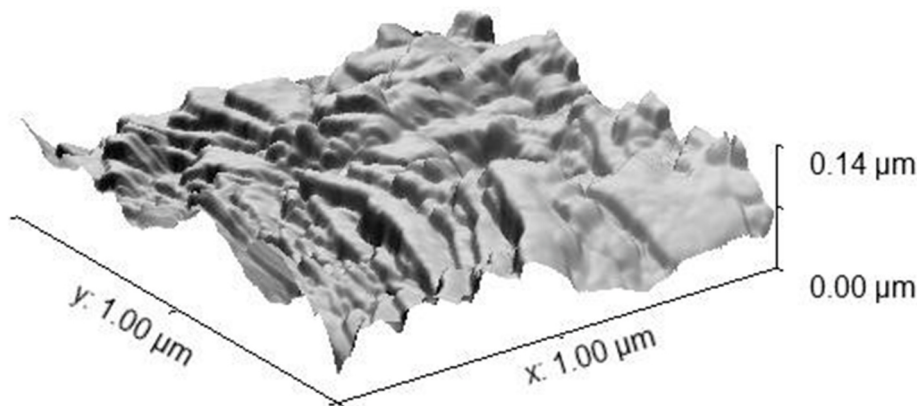


Fig. 15. 3D AFM image from the bulk surface structure of injection molded and etched iPP sample containing 1000 ppm NA21E nucleating agent.

Acknowledgements

The authors would like to express their gratitude to the Ministry of Human Capacities for the New National Excellence program grant. In addition one of the Authors (Alfréd Menyhárd) would like to express his indebtedness for the financial support of János Bolyai Scholarship of the Hungarian Academy of Sciences. Supported by the ÚNKP-20-5-BME-333 New National Excellence Program of the Ministry of Human Capacities and by the János Bolyai Research Scholarship (Grant No. BO/00756/18) of the Hungarian Academy of Sciences. The research reported in this paper and carried out at Budapest University of Technology and Economics has been supported by the NRDI Fund (TKP2020 IES, Grant No. BME-IE-NAT) based on the charter of bolster issued by the NRDI Office under the auspices of the Ministry for Innovation and Technology.

References

- [1] J. Varga, β -modification of isotactic polypropylene: preparation, structure, processing, properties, and application, *J. Macromol. Sci., Part B* 41 (4–6) (2002) 1121–1171.
- [2] R.S. Stein, M.B. Rhodes, Photographic light scattering by polyethylene films, *J. Appl. Phys.* 31 (11) (1960) 1873–1884.
- [3] R.S. Stein, R. Prud'Homme, Origin of polyethylene transparency, *J. Polym. Sci. B Polym. Lett.* 9 (8) (1971) 595–598.
- [4] A. Menyhárd, et al., The influence of nucleus density on optical properties in nucleated isotactic polypropylene, *Eur. Polym. J.* 45 (11) (2009) 3138–3148.
- [5] Z. Horváth, et al., Effect of the molecular structure of the polymer and nucleation on the optical properties of polypropylene homo- and copolymers, *ACS Appl. Mater. Interfaces* 6 (10) (2014) 7456–7463.
- [6] M. Kristiansen, et al., The binary system isotactic polypropylene/bis (3, 4-dimethylbenzylidene) sorbitol: phase behavior, nucleation, and optical properties, *Macromolecules* 36 (14) (2003) 5150–5156.
- [7] E. Nedkov, T. Dobreva, Optical properties of the three polymorphic forms of isotactic polypropylene, *E-Polymers* 2 (1) (2002).
- [8] B. Read, in: G.H. Meeten (Ed.), *Optical Properties of Polymers*, Elsevier Applied Science Publishers Ltd, London, 1986, p. 398, 0-85334-434-5. 1987, Elsevier.
- [9] M.J. Doyle, On the effect of crystallinity on the elastic properties of semicrystalline polyethylene, *Polym. Eng. Sci.* 40 (2) (2000) 330–335.
- [10] B. Crist, C.J. Fisher, P.R. Howard, Mechanical properties of model polyethylenes: tensile elastic modulus and yield stress, *Macromolecules* 22 (4) (1989) 1709–1718.
- [11] R. McCullough, et al., Predictions of limiting mechanical performance for anisotropic crystalline polymers, *Polym. Eng. Sci.* 16 (5) (1976) 371–387.
- [12] R. Boyd, Prediction of polymer crystal structures and properties, in: *Atomistic Modeling of Physical Properties*, Springer, 1994, pp. 1–25.
- [13] J. Halpin, J. Kardos, Moduli of crystalline polymers employing composite theory, *J. Appl. Phys.* 43 (5) (1972) 2235–2241.
- [14] R.H. Boyd, The mechanical moduli of lamellar semicrystalline polymers, *J. Polym. Sci. Polym. Phys. Ed* 21 (4) (1983) 493–504.
- [15] E. Betzig, et al., Breaking the diffraction barrier: optical microscopy on a nanometric scale, *Science* 251 (5000) (1991) 1468–1470.
- [16] L. Sawyer, D.T. Grubb, G.F. Meyers, *Polymer Microscopy*, Springer Science & Business Media, 2008.
- [17] C. Viney, A. Donald, A. Windle, Optical microscopy of banded structures in oriented thermotropic polymers, *J. Mater. Sci.* 18 (4) (1983) 1136–1142.
- [18] J. Bellare, et al., Polarized optical microscopy of anisotropic media: imaging theory and simulation, *J. Colloid Interface Sci.* 136 (2) (1990) 305–326.
- [19] J. Varga, Modification change during spherulitic growth of polypropylene, *Die Angewandte Makromolekulare Chemie: Appl. Macromol. Chem. Phys. Angew. Makromol. Chem.* 104 (1) (1982) 79–87.
- [20] H.E. Keller, Contrast enhancement in light microscopy, *Current protocols in cytometry* (1) (1997), 2.1, 1-2.1. 11.
- [21] F.D. Bloss, *An Introduction to the Methods of Optical Crystallography*, 1961.
- [22] B.E. Sørensen, A revised Michel-Lévy interference colour chart based on first-principles calculations, *Eur. J. Mineral.* 25 (1) (2013) 5–10.
- [23] J. Varga, A. Ille, Y. Fujiwara, $\alpha\beta$ -bifurcation of growth during the spherulitic crystallization of polypropylene, *Period. Polytech. - Chem. Eng.* 34 (4) (1990) 255–271.
- [24] F. Padden Jr., H. Keith, Spherulitic crystallization in polypropylene, *J. Appl. Phys.* 30 (10) (1959) 1479–1484.
- [25] R. Androsch, M.L. Di Lorenzo, C. Schick, Optical microscopy to study crystal nucleation in polymers using a fast scanning chip calorimeter for precise control of the nucleation pathway, *Macromol. Chem. Phys.* 219 (3) (2018) 1700479.
- [26] G. Meeten, *Optical Properties of Polymers*, Elsevier Applied Science Publishers Ltd, Crown House, Linton Road, Barking, Essex IG 11 8 JU, UK, 1986, 1986.
- [27] D.W. Piston, Choosing objective lenses: the importance of numerical aperture and magnification in digital optical microscopy, *Biol. Bull.* 195 (1) (1998) 1–4.
- [28] A. Devillez, S. Lesko, W. Mozer, Cutting tool crater wear measurement with white light interferometry, *Wear* 256 (1–2) (2004) 56–65.
- [29] D. Bassett, Permanganic etching and its insights into crystalline polymers, in: *Developments in Crystalline Polymers*, Springer, 1988, pp. 67–113.
- [30] R. Olley, D. Bassett, An improved permanganic etchant for polyolefins, *Polymer* 23 (12) (1982) 1707–1710.
- [31] B. Ayub, et al., Specimen preparation for electron microscopy: an overview, *Journal of Environment and Life Sciences* 2 (3) (2017) 85–88.
- [32] B. Crist, J.M. Schultz, Polymer spherulites: a critical review, *Prog. Polym. Sci.* 56 (2016) 1–63.
- [33] Q. Guo, *Polymer Morphology: Principles, Characterization, and Processing*, John Wiley & Sons, 2016.
- [34] S. Magonov, *Atomic Force Microscopy in Analysis of Polymers. Encyclopedia of Analytical Chemistry: Applications, Theory and Instrumentation*, 2006.
- [35] S.N. Magonov, D.H. Reneker, Characterization of polymer surfaces with atomic force microscopy, *Annu. Rev. Mater. Sci.* 27 (1) (1997) 175–222.
- [36] D. Trifonova, J. Varga, G.J. Vancso, AFM study of lamellar thickness distributions in high temperature melt-crystallization of β -polypropylene, *Polym. Bull.* 41 (3) (1998) 341–348.
- [37] L. Li, et al., Direct observation of growth of lamellae and spherulites of a semicrystalline polymer by AFM, *Macromolecules* 34 (2) (2001) 316–325.
- [38] J.-J. Zhou, et al., Atomic force microscopy study of the lamellar growth of isotactic polypropylene, *Polymer* 46 (12) (2005) 4077–4087.
- [39] B. Cappella, G. Dietler, Force-distance curves by atomic force microscopy, *Surf. Sci. Rep.* 34 (1–3) (1999) 1–104.
- [40] A. Voss, R.W. Stark, C. Dietl, Surface versus volume properties on the nanoscale: elastomeric polypropylene, *Macromolecules* 47 (15) (2014) 5236–5245.
- [41] C. Ionescu-Zanetti, et al., Semiconductive polymer blends: correlating structure with transport properties at the nanoscale, *Adv. Mater.* 16 (5) (2004) 385–389.
- [42] L.-T. Lee, et al., Current mode atomic force microscopy (C-AFM) study for local electrical characterization of conjugated polymer blends, *Ambio* 41 (2) (2012) 135–137.
- [43] A. Alexeev, J. Loos, M. Koetse, Nanoscale electrical characterization of semiconducting polymer blends by conductive atomic force microscopy (C-AFM), *Ultramicroscopy* 106 (3) (2006) 191–199.
- [44] Z. Horváth, et al., Effect of molecular architecture on the crystalline structure and stiffness of iPP homopolymers: modeling based on annealing experiments, *J. Appl. Polym. Sci.* 130 (5) (2013) 3365–3373.
- [45] H. Awaya, Morphology of different types of isotactic polypropylene spherulites crystallized from melt, *Polymer* 29 (4) (1988) 591–596.
- [46] D. Norton, A. Keller, The spherulitic and lamellar morphology of melt-crystallized isotactic polypropylene, *Polymer* 26 (5) (1985) 704–716.

- [47] J. Varga, Shape of spherulitic boundaries, *Die Angewandte Makromolekulare Chemie: Appl. Macromol. Chem. Phys. Angew. Makromol. Chem.* 112 (1) (1983) 161–172.
- [48] Z. Stachurski, J. Macnicol, The geometry of spherulite boundaries, *Polymer* 39 (23) (1998) 5717–5724.
- [49] R. Stein, W. Chu, Scattering of light by disordered spherulites, *J. Polym. Sci. 2 Polym. Phys.* 8 (7) (1970) 1137–1157.
- [50] S. Clough, J. Van Aartsen, R. Stein, Scattering of light by two-dimensional spherulites, *J. Appl. Phys.* 36 (10) (1965) 3072–3085.
- [51] C. Picot, et al., Interparticle interference in light scattering from spherulitic systems, *Macromolecules* 4 (4) (1971) 467–470.
- [52] R.E. Prud'Homme, R.S. Stein, Light scattering from assemblies of spherulites, *J. Polym. Sci. Polym. Phys. Ed* 11 (7) (1973) 1357–1374.
- [53] M. Motegi, et al., Light-scattering patterns from polyethylene films in relation to spherulitic crystalline texture, *Polym. J.* 1 (2) (1970) 209–221.
- [54] J. Van Aartsen, R.S. Stein, Scattering of light by deformed three-dimensional spherulites, *J. Polym. Sci. 2 Polym. Phys.* 9 (2) (1971) 295–311.
- [55] R.J. Samuels, Small angle light scattering from deformed spherulites. Theory and its experimental verification, in: *Journal of Polymer Science Part C: Polymer Symposia*, Wiley Online Library, 1966.
- [56] D.Y. Yoon, R.S. Stein, A lattice theory of light scattering from disordered spherulites, *J. Polym. Sci. Polym. Phys. Ed* 12 (4) (1974) 763–784.
- [57] J. Boon, G. Challa, D. Van Krevelen, Crystallization kinetics of isotactic polystyrene. I. Spherulitic growth rate, *J. Polym. Sci. 2 Polym. Phys.* 6 (10) (1968) 1791–1801.
- [58] F. Horváth, J. Molnár, A. Menyhárd, Polypropylene nucleation, in: J. Karger-Kocsis, T. Bárány (Eds.), *Polypropylene Handbook: Morphology, Blends and Composites*, Springer International Publishing, Cham, 2019, pp. 121–184.
- [59] J. Molnár, et al., Modeling of light scattering and haze in semicrystalline polymers, *J. Polym. Sci.* 58 (13) (2020) 1787–1795.